Energy Conversion and Management: X 26 (2025) 100906

Contents lists available at ScienceDirect

Energy Conversion and Management: X

journal homepage: www.sciencedirect.com/journal/energy-conversion-and-management-x

Water vapor quantification in raw product gas by THz quantum cascade laser

Florian Johann Müller [a,1,*], Michael Jaidl [b,1], Dominik Theiner [b], Johann Zeitlhofer [a], Florian Benedikt [a,c], Lena Steiner [a], Alexander Bartik [a], Marie Christine Ertl [b], Aaron Maxwell Andrews [d], Gottfried Strasser [d], Stefan Müller [a], Franz Winter [a], Karl Unterrainer [b]

[a] Technische Universität Wien, Faculty of Technical Chemistry, Institute of Chemical, Environmental and Bioscience Engineering, Getreidemarkt 9/166 1060 Vienna, Austria
[b] Technische Universität Wien, Faculty of Electrical Engineering and Information Technology, Photonics Institute, Gußhausstraße 25-29/387 1040 Vienna, Austria
[c] BOKU University, Department of Material Sciences and Process Engineering, Institute of Chemical and Energy Engineering, Muthgasse 107/I 1190 Vienna, Austria
[d] Technische Universität Wien, Faculty of Electrical Engineering and Information Technology, Institute of Solid State Electronics, Gußhausstraße 25-25a 1040 Vienna, Austria

ARTICLE INFO

Keywords:
Online gas analysis
QCL
Gasification
Spectroscopy
Water vapor

ABSTRACT

Online quantification of water vapor in hot and complex gases, like raw product gas from biomass gasification, is essential for process understanding and control. The complex nature of these gases presents many challenges, e. g., band overlap or dust and tar deposits on equipment. Offline measurement by condensing water is labor-intensive and does not provide continuous real-time data. This study introduces a spectroscopic setup consisting of a quantum cascade laser emitting in the far-infrared range, a gas cell heated to around 250 °C, and a pyroelectric detector to quantify water vapor content in real-time. A 1st-order distributed feedback grating ensures single-mode operation of the laser at the desired water absorption line (2.294 THz). This setup was successfully tested for online analysis of raw product gas from steam gasification of waste wood. The average result from the new spectroscopic setup was 45.8 vol-% water vapor content, compared to the condensation measurement, which showed 46.7 vol-% water vapor content. Uncertainty was determined as −0.7 to +1.1 vol-% H_2O. New data from the QCL-based measurement were available every 1 to 5 s, allowing for a better understanding of the process while operating the gasifier. The permanent gas species detected in the raw gas included CO, H_2, CO_2, CH_4, NH_3, and H_2S. Additionally, 4.16 g/Nm^3_{dry} of tar was detected gravimetrically and 31.21 g/Nm^3_{dry} by gas chromatography-mass spectrometry. Measurement continued without issue in this raw, hot product gas from biomass steam gasification for two hours. This work showcases quantum cascade lasers' strong potential for spectroscopy applications in hot and complex gases.

1. Introduction

1.1. Importance of water vapor quantification in hot gases

Climate change has led to greenhouse gas mitigation strategies aiming to limit the global average temperature increase and the resulting severe consequences for the environment and humanity. In 2019, approximately 73 % of net global greenhouse gas emissions came from the sectors of energy (34 %), industry (22 %), and transport (15 %) [1]. Using biomass and waste as feedstock in thermochemical conversion processes, such as pyrolysis, gasification, and combustion, could occupy an essential role in the transition of the already mentioned sectors of energy, industry, and transport and is a critical enabling

* Corresponding author.
E-mail addresses: florian.johann.mueller@tuwien.ac.at (F.J. Müller), michael.jaidl@tuwien.ac.at (M. Jaidl), dominik.theiner@tuwien.ac.at (D. Theiner), johann.zeitlhofer@tuwien.ac.at (J. Zeitlhofer), florian.benedikt@boku.ac.at (F. Benedikt), lena.steiner@tuwien.ac.at (L. Steiner), alexander.bartik@tuwien.ac.at (A. Bartik), marie.christine.ertl@tuwien.ac.at (M.C. Ertl), aaron.andrews@tuwien.ac.at (A.M. Andrews), gottfried.strasser@tuwien.ac.at (G. Strasser), stefan.mueller@tuwien.ac.at (S. Müller), franz.winter@tuwien.ac.at (F. Winter), karl.unterrainer@tuwien.ac.at (K. Unterrainer).
[1] These authors contributed equally to this paper.

https://doi.org/10.1016/j.ecmx.2025.100906
Received 11 October 2024; Received in revised form 15 January 2025; Accepted 31 January 2025
Available online 3 February 2025

Nomenclature

Parameter symbol	Parameter description, unit
A_{CO}	Absorbance of CO, –
c_{Beer}	Concentration of H_2O in the wet gas volume determined by spectroscopy, mol/m^3
c_{CO}	Concentration of CO in the wet gas, mol/m^3
$c_{Condensation}$	Concentration of H_2O in the wet gas determined by condensation, mol/mol
c_{Laser}	Concentration of H_2O in the wet gas determined by spectroscopy, mol/mol
d	Optical path length through the measured medium, m
I	Measured intensity of light at the lock-in amplifier during experiment, V
I_0	Baseline intensity of light at the lock-in amplifier without H_2O in cell, V
$I_{0,N2}$	Baseline intensity of light at the lock-in amplifier with N_2 in cell, V
p	Pressure, Pa
R	Ideal gas constant (8.3144), J/mol/K
T	Temperature, K
ε	Molar extinction coefficient, m^2/mol
Λ	Period length, m
ν	Wave number, 1/cm
σ	Standard deviation of baseline signal, V

Abbreviation	Term
DA	Direct Absorption
DFB	Dual Fluidized Bed
FTIR	Fourier-Transform InfraRed
GATS	GATS, Inc.: Small aerospace company
GC-FID	Gas Chromatography – Flame Ionization Detector
GC–MS	Gas Chromatography – Mass Spectometry
IR-LAS	InfraRed Laser-Absorption Spectroscopy
NDIR	Non-Dispersive InfraRed
OF-CEAS	Optical Feedback Cavity-Enhanced Absorption Spectroscopy
QCL	Quantum Cascade Laser
SEM	Scanning Electron Microscopy
SNG	Synthetic Natural Gas
TCD	Thermal ConDuctivity
TDLAS	Tunable Diode Laser Absorption Spectrometry
VMR	Volume Mixing Ratio
WMS	Wavelength Modulation Spectroscopy

technology for various defossilization and negative emission technologies [2]. Switching the fuel from fossil to biomass and adapting the process by capturing CO_2 in situ, e.g., with chemical looping or in the flue gas, can lead to a so-called net-negative emission process [3]. In several industrial processes, e.g., thermochemical fuel conversion, energy generation, chemical production, and steel or concrete production, measuring the water vapor content in hot gases is crucial in process control. The variability of waste and biomass feedstocks, e.g., variations in moisture content resulting from changes in harvesting conditions [4], presents additional challenges for process control and optimization. The heterogeneity of these alternative feedstocks further increases the importance of accurate and real-time water vapor content measurement for assessing process efficiency, optimizing operational parameters, and ensuring safe operation.

1.2. Challenges for water vapor quantification on the application example of raw product gas

Biomass steam gasification is investigated in this new work as an exemplary technology, notorious for presenting many challenges to water vapor measurement in raw and hot gas. A successful demonstration of water vapor quantification in this process would be promising for a future transfer of this technology into other industries, where gas compositions are often less challenging to measure. In gasification, the organic feedstock is not fully oxidized but converted with a gasifying agent such as steam, under-stoichiometric addition of air or oxygen, or CO_2 into so-called raw product gas [5]. The main components of the raw product gas are hydrogen, carbon monoxide, carbon dioxide, methane, steam, and C_2 and C_3 permanent gases. Raw, in this context, refers to the gas before it is cleaned and still contains condensable species and possibly particles. The product gas can be further conditioned and prepared for the synthesis of various products; hence, the cleaned version is called synthesis gas or, in short, syngas. Syngas can be converted and refined to gaseous energy carriers, transportation fuels, and other chemical products such as Fischer-Tropsch products [6], synthetic natural gas (SNG) [7], hydrogen [8] and many more [9]. Biomass gasification using a dual-fluidized bed (DFB) reactor design with around 100 kW_{th} biomass input has been a central research interest at TU Wien and is described in numerous publications, e.g., [7,8,10]. The DFB design consists of two interconnected reactors, where one generates the raw product gas in an endothermic process. At the same time, the other provides heat for the endothermic gasification by combustion of additional feedstock. DFB reactors for biomass gasification are also relevant at larger scales, e.g., as shown by the GoBiGas plant that produced 20 MW of SNG until decommissioning in 2018 [11]. A good solution for measuring water vapor in the raw product gas from these reactors is missing, which is explained by the wide range of compounds in the gas.

The composition of raw product gas, especially its water vapor content, is heavily influenced by the amount and type of gasifying agent, the fuel water content, and the operating temperature [12]. The product gas's main gas composition, the so-called gas matrix, can vary significantly, complicating the analytics task. Common raw product gas impurities include particulate matter like dust and char particles, heavy organic compounds, and other species such as NH_3, H_2S, and HCl, which depend on the fuel used [13]. The formation of tar in the raw product gas is one of the significant challenges in the thermochemical conversion of biomass and waste through gasification. Several definitions for the term "tar" exist. The definitions for tar used in this work follow the pre-standard CEN/TS 15439:2006, which defines tar as a "generic term for the totality of all organic compounds present in the product gas from gasification, with the exception of gaseous hydrocarbons (C1 to C6)" [14]. Tar can condense at temperatures around 200 °C and ambient pressure, which leads to significant issues regarding downstream equipment, e.g., particulate filters or heat exchangers [10]. For analytics in raw product gas, tar poses various problems for a wide range of gas analyzers, e.g., band overlap and fouling [15]. These other species complicate the water quantification task, and water vapor in raw product gas can also have detrimental effects on other analyses. Kleinhappl [16] discussed these problems, which include the dilution of solvents, phase separation, slip of non-polar fractions during sampling, ice formation, baseline instabilities in gas chromatography-flame ionization detectors (GC-FID), or discrimination during evaporation in GC injectors.

1.3. Established water vapor quantification technologies

Measuring the main product gas components in the cold and water-free state is sufficiently solved, e.g., after appropriate gas purification, combustion with subsequent cooling, or gas sampling equipped with condensation and filters. Measuring raw gas in the hot state is much

more complicated, and no method has established itself as a standard for online water vapor quantification in raw and hot gases with complex compositions. Aranda Almansa et al. [15] report the state-of-the-art measuring procedures for water quantification in raw product gas and their shortcomings: Offline sampling methods like gravimetric quantification and solid phase adsorption are low-cost but suffer from manual procedure issues and often cannot accurately reflect dynamic system behavior. Online and semi-online sampling via chromatography face co-adsorption and maintenance challenges. Real-time methods, including hygrometers, acoustic measurement, and spectrometry, are costly and often affected by dust, tar deposits, and band overlapping. Further challenges include the strong light attenuation of product gas, high temperatures, the significant number of different compounds, and especially the negative effect of particulate matter in the gas, lowering the possible optical path length if visible or near-infrared wavelengths are used [17].

The most widespread spectroscopic devices for combustion and gasification gas analysis are infrared laser-absorption spectrometers (IR-LAS), as described in several reviews [18,19]. IR-LAS instruments use the absorption and emission effects when the spacing between two discrete rotational-vibrational states equals the photon energy [18]. The density or concentration of the analyzed species can be derived from the total absorbed or emitted radiation. Most devices use light sources in the near- or mid-infrared domain [18]. Tunable laser diodes are widespread light sources, and tunable diode laser absorption spectroscopy (TDLAS) has been used extensively for quantitative online and in situ real-time combustion and gasification diagnostics [18,19]. Multiple signal evaluation strategies have been described and compared in the literature and can be summarized into two groups: direct absorption (DA) and wavelength modulation spectroscopy (WMS) [18–20]. DA systems are generally simpler to build and calibrate but less sensitive and resistant to noise [21]. Sepman et al. have demonstrated in several studies the use of TDLAS for in situ H_2O measurement in the reactor core of a biomass gasifier [22–25]. These studies showed reliable performance even under high-temperature and high-soot conditions. A TDLAS sensor near 4350 cm^{-1} was developed for in situ CO, H_2O, and soot concentration measurements in a pilot-scale gasifier's reactor core, achieving temperature-insensitive species quantification from 1000 K to 1900 K [22]. H_2O quantification uncertainties were reported as better than 10 % compared to calculations [24] and 20 % compared to micro-gas chromatograph data [22]. Sur et al. have shown that TDLAS can also be applied in pressurized gasifiers [26].[17,2717].

Other techniques for online or in situ determination of H_2O content include Raman spectroscopy (RS) [28], acoustic measurements [29], humidity meters [30], soft sensors [31] and others, not all of which are explained in detail here. RS is highly flexible and can be used for various analysis tasks in the thermochemical processing of biomass, coal, and waste [28]. RS is based on inelastic scattering of light, where the frequency of photons is shifted due to interaction with molecular vibrations [32]. Raman spectroscopy has been demonstrated for H_2O quantification in biogas [33] and biomass gasification [34] applications. However, Xu et al. [28] note in their review that Raman spectroscopy has rarely been used to analyze gas components. They suggest that this is caused by the low density and Raman cross-section of gases, making it challenging to obtain high-quality Raman spectra. Karellas and Karl also noted that high gas flows or tar contents lead to intense background signals, obscuring the Raman peaks of other gas compounds [34]. An online estimation method was recently proposed by TUW, consisting of a soft sensor that estimates raw product gas composition based on a Hammerstein model and two extended Karman filters [31]. However, this method requires training on historical data for the specific plant and relies on other measurements, such as gas chromatography, which presents challenges for new or dynamic systems.

1.4. Water vapor measurement with a THz laser

The present work introduces a quantum cascade laser emitting light in the far-infrared domain at terahertz frequencies for continuous water vapor measurement in hot and raw product gas from gasification. As summarized in a recent review [35], lasers emitting in the THz spectral region (commonly defined as the frequency range 0.1 – 10 THz) have been tested for water detection in various applications [35]. Although the review describes a significant amount of research in this field, there is little information on high-temperature systems with complex gases from industrial applications. In general, water vapor has various absorption lines at sufficiently high temperatures to avoid tar condensation [30], with some even stronger at high-temperature than at room temperature [36]. Additionally, compared to other lasers used for spectroscopy in the visible, near- or mid-infrared spectral domains, THz lasers have longer wavelengths. These longer wavelengths make them more resistant to Mie scattering [37,38] from dust, which is typically present in off-gas flows from industrial applications [30,36]. Most organic compounds and inorganic ions absorb in the near- or mid-infrared region between 400 – 4000 cm^{-1}, which is around 12 – 120 THz [17]. For these reasons, a THz laser in the far-infrared region is expected to be more robust against band overlapping with the various organic compounds in gasification processes.

Song et al. investigated THz lasers for their ability to measure water vapor content in N_2/H_2O mixtures at 773 K. They found three absorption peaks at 557 GHz, 658 GHz, and 752 GHz, where water vapor content could be quantified using a gas cell with a length of 1 m [36]. This work is promising; however, the tests were conducted in batches by feeding H_2O with syringes into the cell, which otherwise only contained nitrogen from a gas bottle. Therefore, this test did not include the additional challenges posed by dust and various permanent and condensable gases mixed with water vapor in the raw product gas.

Bidgoli et al. investigated a spectroscopic setup for measuring water vapor from gasification [30]. They did screenings and statistical analysis with lasers between 300 and 500 GHz and a gas cell with a length of 1.6 m. They concluded that THz gas spectroscopy could efficiently provide real-time data on water vapor in complex gas mixtures containing dust particles and tar components. However, their publication had significant trouble correlating the measured signal to a volume mixing ratio (VMR) of water because of unclear temperatures in the gas cell. The extensive length of the cell worsened this problem.

This present work uses a similar spectroscopic setup as [30] with hot (~250 °C) gas flowing through the measurement cell to detect water vapor and measure its concentration by selective absorption of light emitted by a quantum cascade laser (QCL). A first experimental campaign was conducted with synthetically prepared gas mixtures. An advanced setup was used to measure raw product gas from biomass steam gasification. THz QCLs are electrically driven lasers with a semiconductor heterostructure [39]. Their advantages include a compact design, high output powers, and frequency tunability. The QCL in this new setup allows for a gas cell with a short beam path of only 86 mm, drastically reducing the cell temperature variations that [30] observed and making the setup more compact by reducing the gas cell length by over 90 %. This design is investigated in the present work for online analysis of water vapor. Raw and hot product gas from biomass steam gasification is measured and used as an example of a potential application scenario with significant challenges for online measurement.

2. Theory and calculation

2.1. Selection of laser frequency

Viveros Salazar et al. summarized the necessary steps and considerations to select a suitable laser frequency [20]. Computational prediction of absorption characteristics demands a line list including information such as wavelength, line strength, and collision-broadening

effects for each chemical species. In this work, the Spectral Calculator developed by GATS, Inc. was used to calculate absorption and transmittance at specific wave numbers, temperatures, gas cell lengths, and volumetric mixing ratios [40]. This calculator uses the HITRAN2020 database [41] as a line list to perform line-by-line molecular absorption calculations based on the line-by-line model in the LinePak^{TM} library [42]. The spectral calculator includes weighted air- and self-broadened halfwidths depending on pressure and temperature from the HITRAN2020 database to calculate the line shape. This method yields a combination of Doppler and Lorentz broadening, resulting in the more general Voigt profile.

The next step for laser frequency selection is estimating operating conditions [17,20]. Essential conditions to estimate include temperature, pressure, and other chemical components surrounding the measured species, which might contribute to absorption. Atmospheric pressure was selected for measurement since TUW usually does not pressurize their gasifiers. A temperature range of 100 – 400 °C was considered appropriate to retain some flexibility in operation and avoid the condensation of water and tar in the cell. The concentration of gaseous main components and impurities in raw product gas heavily depends on fuel composition [43]. In addition, raw product gas can contain various tars, fly char, and dust, for which no information is available from the Spectral Calculator or in the HITRAN database. Bidgoli et al. [30] did not report a significant influence of these components in their work with laser frequencies between 300 and 500 GHz. A hot gas filter was used to reduce the particle density in the beam path in our work. Furthermore, the size of most particles after the gasification reactor's filter system in the present work is well below the laser wavelength of 130.69 μm. Therefore, particles are not assumed to impede the transmission of laser light significantly [37,38]. This work uses the simplification that no interaction between the laser light and any solid particles or molecules other than H_2O or CO occurs.

Once absorption theory and operating conditions are established, the selection of a laser frequency needs to achieve sufficient selectivity over other components and absorption signal strength for detection [17,20]. Viveros Salazar et al. suggest a 10 – 90 % laser transmission for sensitive measurements [20]. The laser transmission depends on the beam path length (see ***Section 2.2***). Our work also aimed to select a laser frequency at which the beam path could be relatively short while achieving the 10 – 90 % transmission criteria. A short beam path allows for a more compact setup, promising multiple benefits such as transportability and less temperature variation inside the measurement cell. Another important criterium for laser frequency selection is the availability of a suitable laser.

Data from the Spectral Calculator were used to identify 2.294 THz, respectively, a wave number of 76.52 cm^{-1}, as a suitable water absorption frequency line for analysis of raw product gas from biomass gasification among available THz QCLs with sufficient power output. Other main components in typical product gas show comparably weak absorption at this frequency. Absorption values of the predominant product gas species from gasification are listed in Table 1. These values are calculated at 250 °C and 1.013 bar_a for a cell with 86 mm optical path length, approximating the conditions used in this work. The absorption of water vapor at the chosen wave number is much stronger than the absorption of the following closest species, carbon monoxide, at a similar concentration. Other species absorb this light even weaker by multiple orders of magnitude. Among impurities, NH_3 and HCN are calculated to show the highest absorption at typical gas concentrations from biomass gasification in a DFB reactor [44]. Their absorption at the highest typical concentrations is similar to the absorption of pure CO.

The absorption of H_2O at 2.294 THz is calculated between 0.2 – 96 %, corresponding to 0.1 – 100 vol-% H_2O in the gas cell. The laser transmission is between 10 – 90 % when the H_2O concentration is approximately 5 – 80 vol-% in the gas cell, suggesting that sensitive measurement is possible over a wide range of H_2O concentrations (Fig. 1b). In contrast, even at their highest considered VMR, no other gas component in typical raw product gas from DFB gasification is estimated at more than 4 % absorption, with average absorption being even lower by orders of magnitude. Furthermore, the absorption of CO can be dynamically excluded from the measurement using dry gas composition data from other measurements, e.g., non-dispersive infrared (NDIR) measurement. In summary, the frequency of 2.294 THz allows measurement with minimal cross-sensitivity for other gas components. This design allows the laser to quantify water vapor over a wide range of raw gas compositions.

Fig. 1a shows 16 Fourier-transform infrared spectrometer measurements, experimentally confirming that the laser emits light at the design frequency of 2.294 THz. The spectrometer's resolution of ±0.08 cm^{-1} is defined by the path difference of the interferometer arms and leaves some margin of error, which is reflected in Fig. 1a. Spectra calculated for this laser frequency by the Spectral Calculator at various H_2O concentrations (Fig. 1b) and temperatures (Fig. 1c) are examples of feasible operating conditions. Fig. 1b shows that H_2O concentrations can be well differentiated over a wide range of water vapor concentrations at 250 °C. Fig. 1c demonstrates that H_2O still absorbs at 400 °C, enabling the measurement in hot and raw gas to avoid extensive fouling from tar

Table 1
Absorption of the typical raw product gas components and impurities from biomass gasification [45–47] as calculated by the Spectral Calculator [40] at λ = 2.294 THz ($\nu \approx 76.52$ cm^{-1}) for a gas cell with 8.6 cm length, 1013.25 mbar pressure, 523.15 K. The abbreviation "B.L." means "below limit", which was arbitrarily chosen at 1E-06.

	Considered gas concentration	Absorption at the lowest considered concentration	Absorption at the highest considered concentration
Main component	**vol-%**	–	–
H_2O	0.1 – 100	1.7E-03	9.6E-01
N_2	0.1 – 100	B.L.	B.L.
H_2	0.1 – 100	B.L.	B.L.
CH_4	0.1 – 100	B.L.	3.9E-05
C_2H_4	0.1 – 100	B.L.	B.L.
CO	0.1 – 100	3.5E-05	3.7E-02
CO_2	0.1 – 100	B.L.	B.L.
O_2	0.1 – 100	B.L.	1.2E-06
Impurity	**ppm (vol.)**	–	–
NH_3	1,000 – 100,000	1.3E-04	1.8E-02
HCN	10 – 1,000	3.3E-04	3.3E-02
H_2S	10 – 1,000	2.5E-06	2.5E-04
COS	0.1 – 100	B.L.	B.L.
HCl	0.1 – 100	B.L.	2.7E-06
NO	10 – 1,000	B.L.	5.6E-06
N_2O	0.1 – 100	B.L.	B.L.
NO_2	0.01 – 1	B.L.	B.L.
SO_2	0.1 – 100	B.L.	5.1E-04

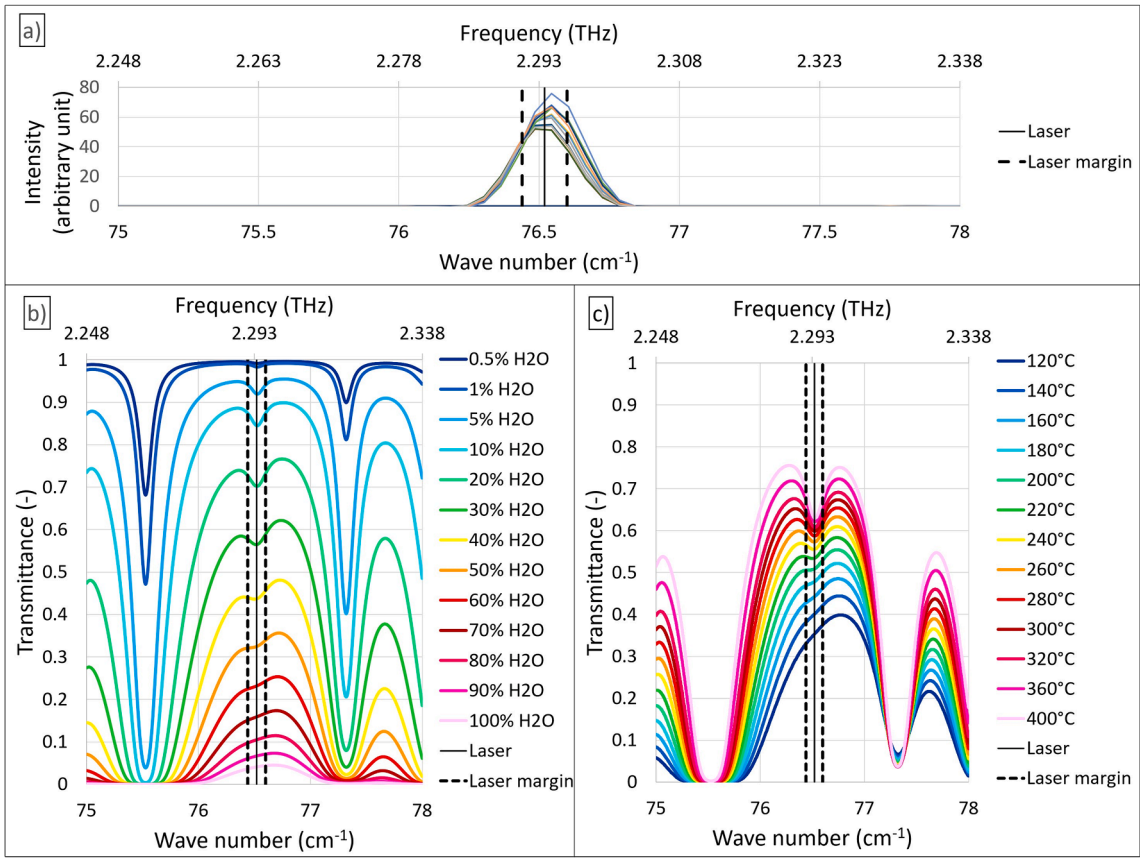

Fig. 1. A) Experimentally found laser spectra with margins of error resulting from discretized measurements. b-) and c): transmittance calculated with data from the spectral calculator [40] for various volume mixing ratios of H_2O at 250 °C (b), various temperatures at 30 vol-% H_2O (c).

condensation. Transmittance at the example water vapor concentration of 30 vol-% is similar from 250 – 400 °C, showing robustness against temperature deviations in the measured gas in this range.

2.2. Measurement of water vapor content

Fixed-wavelength direct absorption spectroscopy is used in this work to detect H_2O. The H_2O concentration c_{Laser} is calculated from Beer-Lambert's law (***Eq. (1)***), which describes the absorption as a function of line strength, line shape, gas pressure, the concentration of the gas in the light's path, and the optical path length [17]. Molar extinction coefficient data (ε), which summarize several of these dependencies, are discussed for H_2O and CO in ***Section 2.3***. The absorption is calculated from the detected laser intensity during an experiment (I) and a baseline intensity with no H_2O in the cell (I_0). Beer-Lambert's law typically expresses the concentration in mol/m^3 (here termed c_{Beer} for differentiation). The ideal gas law accounts for the gas' thermal expansion. The H_2O concentration c_{Laser} in mol/mol or m^3/m^3 is calculated by comparing c_{Beer} to the total gas per volume at the temperature T and pressure p (***Eq. (2)***). The temperature over the integration path is assumed as constant. This assumption is justified by preheating the gas in the sampling line and gas cell with the same heating coil and keeping the optical path length short at only 8.6 cm. The baseline intensity in N_2 atmosphere ($I_{0,N2}$) is determined shortly before experiments. The absorption of gases other than N_2, specifically CO, lowers the baseline intensity I_0 during the experiment with gas mixtures compared to $I_{0,N2}$. I_0 is not available as measurement during the experiments and is instead calculated from $I_{0,N2}$ (***Eq. (3)***). The CO absorbance (A_{CO}) is also calculated from Beer-Lambert's law using the wet CO gas concentration (c_{CO}) (***Eq. (4)***). Dry gas composition data from non-dispersive infrared (NDIR) measurement (***Section 3.3.2***) are implemented in the solving algorithm (***Section 2.3***, Appendix A) to derive c_{CO}. The cell's inner optical path length through the measured gas has the length d.

$$c_{Beer} = \frac{log_{10}\left(\frac{I_0}{I}\right)}{\varepsilon_{H2O} \cdot d} \tag{1}$$

$$c_{Laser} = \frac{R \cdot T \cdot log_{10}\left(\frac{I_0}{I}\right)}{\varepsilon_{H2O} \cdot d \cdot p} \tag{2}$$

$$I_0 = I_{0,N2} \cdot 10^{-A_{CO}} \tag{3}$$

$$A_{CO} = \frac{c_{CO} \cdot \varepsilon_{CO} \cdot d \cdot p}{R \cdot T} = log_{10}\left(\frac{I_{0,N2}}{I_0}\right) \tag{4}$$

2.3. Molar extinction coefficient ε and solving algorithm

The molar extinction coefficients of water vapor ε_{H2O} and CO ε_{CO} are determined from transmittance data given by the Spectral Calculator [48] for a cell with 86 mm optical path length at a pressure of 1013.25 mbar. Three wave numbers were considered: the design laser wave number and its experimentally found upper and lower margins of error: 76.52±0.08 cm^{-1}. These data include VMR for H_2O and CO between 0.1 – 100 vol-% and temperatures between 110 – 400 °C, representing the target operating conditions. ***Eq. (2)*** was rearranged to solve for ε_{H2O} and ε_{CO}. While ε_{CO} was found to be 1–2 orders of magnitude below ε_{H2O} and relatively constant at a higher wave number, ε_{H2O} depends on the temperature, water concentration, and wave number (Fig. 2).

At high temperatures and low water concentrations, the differences in ε_{H2O} for the investigated laser frequencies are sizeable, which is

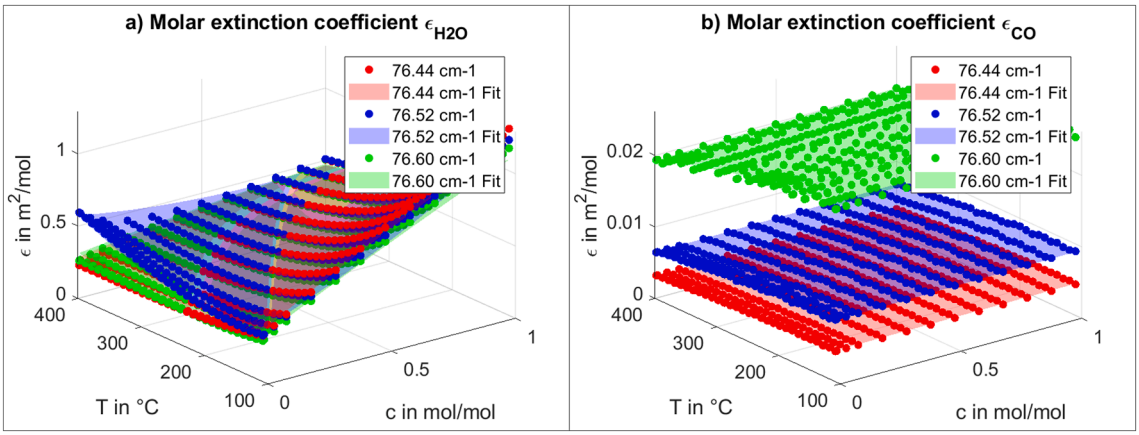

Fig. 2. Molar extinction coefficients fit (surface) based on data from Spectral Calculator (data points). A) H_2O, b) CO.

reflected as uncertainty in the results of this work. The molar extinction coefficient's dependence on the temperature can be accounted for using temperature data from the measurement inside the cell. The molar extinction coefficient's dependence on the molar H_2O concentration means that ***Eq. (2)*** needs to be solved iteratively. For this reason, a solving algorithm is adopted to determine c_{Laser} (Appendix A). Data are typically measured and evaluated internally at an interval of 1 s. Moving average data with a window size of 60 s are given as output to reduce noise. The NDIR measurement can be connected to the QCL setup's solving algorithm, adjusting the signal baseline for CO cross-absorption in real-time.

3. Material and methods

3.1. QCL-based H_2O measurement

3.1.1. THz QCL characteristics

The active region of the used laser consists of a bound-to-continuum design in the GaAs/AlGaAs-material system [49]. A picture taken by scanning electron microscopy (SEM) is included in Appendix B.

The center frequency of the gain bandwidth is at 2.3 THz. The heterostructure was processed into double-metal waveguides. A 1st-order distributed feedback grating [50] was employed on the 2.5 mm long ridge waveguide to ensure single-mode operation at the desired water absorption line (2.294 THz, 130.69 μm, 76.52 cm^{-1}). The emission wavelength can be tuned slightly by changing the operation temperature. Different gratings with varying periods were tested to determine the best fitting to the absorption line. In the first campaign, a laser with a period of $\Lambda = 19.272$ μm was used, where the entire width of the ridge is 60 μm, and the setback is 10 μm. The second campaign used a device with an adjusted period of $\Lambda = 19.22$ μm. This adaptation was employed to reduce the required wavelength shift by temperature. This way, the operating temperature could be lowered, and the output power could be enhanced. A spectrometer with a resolution of ±0.08 cm^{-1} was used to check the wave number of the processed laser. The THz QCL is operated at a temperature of 90 K (resp. 70 K in the second campaign), enabled by a commercial Stirling cooler with a power of 70 W. A vacuum pump provides a pressure of $1.6 \bullet 10^{-6}$ mbar within the laser housing. The operating temperature is monitored by a PT100 sensor and is stabilized by a high-performance resistor used as a heater. Both are attached to the cold finger of the cryostat. Electrical pulses drive the QCL with a repetition rate of 100 kHz and a pulse length of 7 resp. 9.5 μs (duty cycle: 70 resp. 95 %, voltage pulse generator: Agilent 8114A), which are again modulated with a gating frequency of 13 Hz (frequency generator: Agilent 33220A). This gating frequency enables signal detection at the pyroelectric detector, which is comparatively slow (bandwidth ~ 100 Hz).

3.1.2. Gas cell setup

The main components of the spectroscopy setup include the light source (THz QCL), the gas cell, the pyroelectric detector, and two parabolic mirrors. A sketch of these components' arrangement and the light's corresponding beam path is shown in Fig. 3a. The measurement cell is made from alumina (Fig. 3b). The cell is a hollow cylinder separated into three closed-off sections by quartz glass windows with a width of 1 mm each. The outer sections are flushed with nitrogen at 0.5 NL/min to minimize the danger of the leakage of dangerous gas components like CO into the ambient. The flushing also lowers the outer quartz glass windows' temperature, protecting the pyroelectric detector from overload. A downside of this flushing is the increased risk of tar condensation in the central section caused by lower temperatures at the windows. The central section has an inner length of 86 mm and contains the measured gas sample. Trace heating was installed around the measurement cell to prevent condensation.

A prototype for the measurement cell without integrated temperature measurement was used during the first campaign with synthetically prepared gas mixtures from bottled gas. The temperature in the cell during these tests was measured with an infrared sensor by Beha-Amprobe on the cell's outside wall. An uncertainty of ±10 °C compared to the temperature in the cell was assumed for these temperature measurements with the following reasoning: First, no water condensation inside the cell was observed at 110 °C outside wall temperature, suggesting that the maximum negative deviation could have been −10 °C. Second, alumina's high heat conductivity and the small gas cell size suggest a relatively good heat distribution where even local hotspots are unlikely to exceed +10 °C. An advanced cell design, including a thermocouple type K and improved heating and insulation around the cell, was used for the second campaign measuring hot and raw product gas from a gasifier. Pictures of the advanced setup are available in Appendix B.

In the setup, the first parabolic mirror collects the laser beam emitted from the device, converts it to a parallel beam, and guides it to the measurement cell. The second parabolic mirror focuses the THz light from the measurement cell onto the pyroelectric detector. The detector measures the laser beam's intensity. To allow for the detection of the THz light by the pyroelectric detector and read out by a lock-in amplifier (Stanford Research SR830), the THz QCL is driven by a double-modulated voltage signal (see ***Section 3.1.1***).

3.2. Gas production

This work describes two experimental campaigns. The setup prototype was used to investigate synthetically prepared gas mixtures and validate the basic functionality. The advanced setup was tested in a second campaign with raw product gas produced via steam gasification

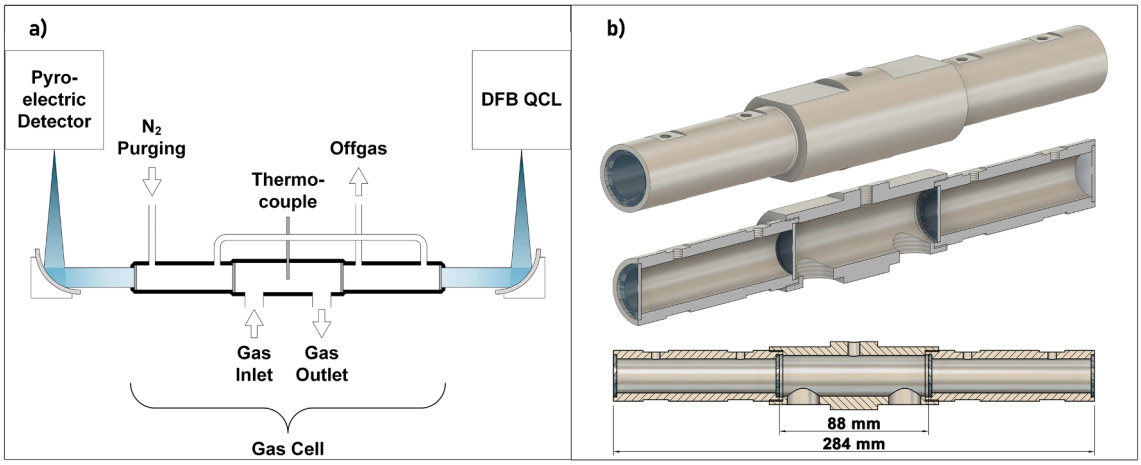

Fig. 3. Gas measurement cell. a) Sketch of gas and light pathways ("DFB QCL"=distributed feedback quantum cascade laser) and b) 3D design drawing.

of waste wood in a DFB gasifier. More detailed information on the gas sampling and measurements is given in ***Section 3.3***.

3.2.1. First campaign: Synthetically prepared gas mixtures

A gas preparation unit consisting of bottled gases, mass flow controllers (MFC), an electrically heated water evaporator, and a water pump was used to prepare the synthetic gas mixtures for the first campaign. Fig. 4 shows a basic flowsheet of the setup, with only one gas sampling point alternating between the H_2O condensation or the H_2O laser and dry product gas measurements. The pipes downstream of the evaporator were electrically heated to approximately 200 °C to prevent condensation.

Table 2 lists the target values of the dry gas composition for the permanent gases and the varying H_2O content. The carrier gas for MIX 1–3 is nitrogen, while the carrier gas for MIX 4–6 resembles a typical product gas from fixed-bed air gasification [51]. The target water vapor content ranges between 10 and 50 vol-%. The liquid water flow to the evaporator was only controlled by the pump, and so the actual values might have differed.

3.2.2. Second campaign: DFB gasification

A 100 kW_{th} DFB gasification pilot plant at TU Wien was used to produce raw product gas. The DFB pilot plant and the SNG process chain have been described in various publications by TU Wien [7,44,46,52]. As the gasification process is not within the scope of this study, only a summary is given here.

A basic flowsheet of the setup is shown in Fig. 5, including the most relevant temperatures during the investigated gasification campaign's stationary operation. DFB gasification is built on the principle of two interconnected fluidized beds. In the gasification reactor, biomass is gasified with steam or other gasification agents like CO_2 at approximately 800 °C, producing a raw product gas. Residual, ungasified char is transported to the combustion reactor with a circulating bed material. In the combustion reactor, char is combusted with air, and the hot bed material is transported back to the gasification reactor to drive the endothermic gasification reactions. The raw product gas leaves the gasifier via a cyclone and a radiation cooler where particles are reduced, and cooling occurs. A hot gas filter further reduces dust concentrations before the product gas is directed to a downstream synthetic natural gas process chain. For the investigated gasification campaign, 22.5 kg/h waste wood was gasified with steam at approximately 777 °C with an 80/20 wt-% mixture of olivine/limestone as bed material.

Table 2
Target gas compositions used for experiments with synthetically premixed gas.

Experiment	N_2	CO	CO_2	H_2	CH_4	H_2O
	vol-%$_{dry}$	vol-%$_{dry}$	vol-%$_{dry}$	vol-%$_{dry}$	vol-%$_{dry}$	vol-%
MIX 1	100	–	–	–	–	25.0
MIX 2	100	–	–	–	–	10.0
MIX 3	100	–	–	–	–	50.0
MIX 4	45	20	13.3	19.25	2.45	42.5
MIX 5	45	20	13.3	19.25	2.45	50.0
MIX 6	45	20	13.3	19.25	2.45	35.0

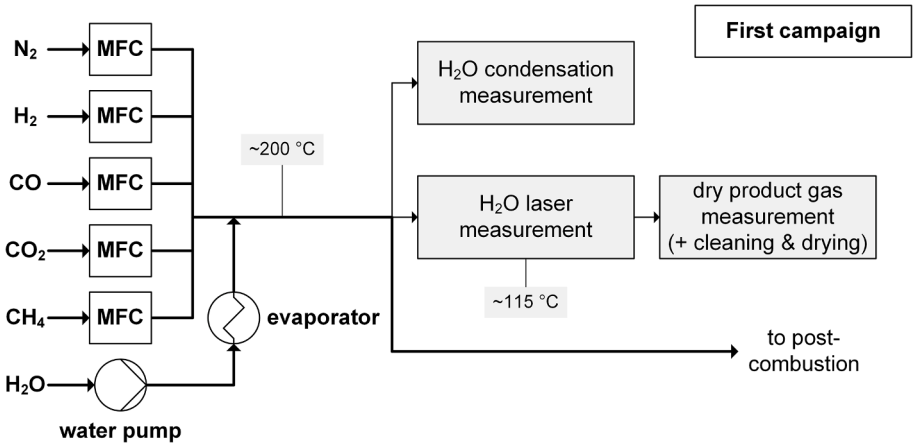

Fig. 4. Basic flowsheet of the gas preparation unit for synthetic mixtures.

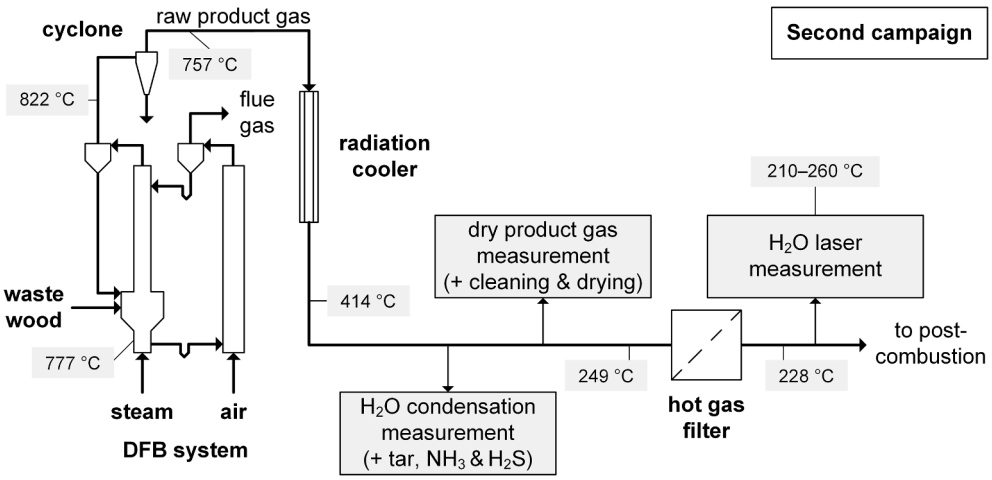

Fig. 5. Basic flowsheet of the raw product gas preparation from a 100 kW_{th} DFB gasifier.

3.3. Gas sampling and conditioning

This chapter describes the differences in sampling procedures for the various measurements conducted in this work.

3.3.1. Condensation and dissolution measurements

Water vapor, tar, NH_3, and H_2S content can be measured discontinuously by condensing or dissolving them and relating the sampled amount to the dry carrier gas flow through the sampling line. This methodology is well established and is the current standard used during gasification experiments at TU Wien. Such results have been reported in various publications, e.g., [7,10], and are based on the procedure described in the tar guideline [14]. The resulting H_2O data is termed $c_{Condensation}$ in this work.

Only one gas sampling point was available during the first campaign with synthetic gas mixtures, resulting in an alternating collection of water vapor quantification data by laser and condensation. On the contrary, individual sampling points for each H_2O measurement and the dry product gas measurement were available during the second campaign. The second campaign also included tar measurements during the H_2O condensation measurement. Furthermore, NH_3 and H_2S content in the raw product gas were quantified at the same sampling point with slightly adjusted methods.

The sampling setup for discontinuous tar and water vapor content measurement is depicted in Fig. 6. A heated cyclone and glass-wool stuffed filter cartridge removed particles that could otherwise distort the measurement. Condensate was collected in chilled Impinger bottles filled with toluene in a cryostat filled with glycol at −8 °C. A diaphragm pump drew a sample gas stream through the cooled toluene in the Impinger bottles and a bellows gas meter measured the dry gas volume. The standard volume of sampled dry gas was calculated from the bellows gas meter's readout via the ideal gas law, using an integrated temperature measurement and ambient pressure data from a nearby weather station run by GeoSphere Austria [53]. The liquid mixture was transferred from the bottles into a separating funnel, where the denser water phase was collected at the bottom. This phase was separated into a measuring cylinder to determine the total volume of the liquid water collected. Depending on the estimated water content, sampling was done for 12 – 18 min.

Aqueous solvents replaced toluene to collect NH_3 and H_2S, for which the cryostat was tempered to +2 °C. NH_3 was captured in a 0.05 M H_2SO_4 and H_2S in 35 wt-% KOH. H_2S was determined by titration and NH_3 by ion chromatography from these aqueous samples. The exact procedure is further detailed in [54].

Gravimetric tar content is determined from the mass of solid residues after solvent distillation and evaporation of a sub-sample [14]. Another sub-sample of the tar-toluene mixture was further analyzed by coupled gas chromatography-mass spectrometry (GC–MS) to determine the tar concentration and composition. These data were used to derive the tar dew point. The dew point for these mixtures can be estimated from vapor/liquid equilibrium calculations for single components [56], followed by the application of Raoult's law [57].

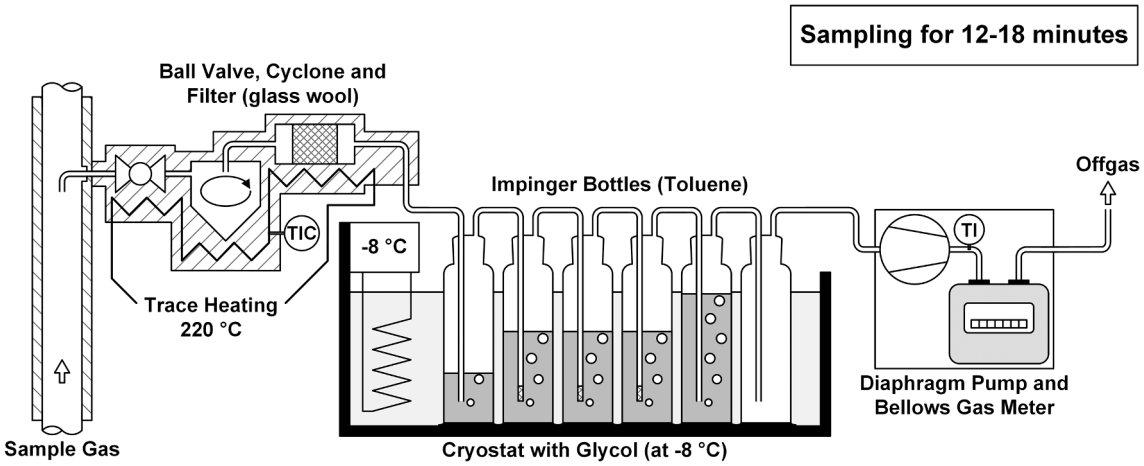

Fig. 6. Discontinuous tar and H_2O condensation measurement via condensation in toluene, adjusted from [55].

3.3.2. Spectroscopic measurements

The new QCL-based H_2O measurement and Emerson's NGA2000 dry gas analyzer were used to collect data continuously. Gas was sampled from a single port, and both spectroscopic measurements were serialized during the first campaign (Fig. 7). The second campaign with raw product gas used two separate sampling lines: One without trace heating for the dry gas measurement and one without dry gas analyzer for the QCL-based H_2O measurement. Fig. 7 shows the combined installation layout. The sampling point for the H_2O laser measurement during the second campaign was placed after the inline hot gas filter to avoid high particle loads without installing another particle separation system.

The sampled gas was sucked through a section with trace heating, which covered the sampling line and the gas cell's central section. A temperature measurement located on the sampling line's outside wall was used for temperature control, which was set to 150 °C in the first campaign and 315 °C in the second campaign. Chilled impinger bottles filled with heating oil, followed by a glass-wool stuffed filter cartridge, were used to dry and clean the gas before the diaphragm pump. Finally, the gas stream was directed through the dry gas analyzer. This dry gas analyzer combines NDIR spectroscopy to measure CO, CO_2, and CH_4, paramagnetic O_2 analysis, and a thermal conductivity (TCD) sensor to measure H_2.

4. Results

4.1. First experimental campaign measuring synthetically prepared gas mixtures with setup prototype

Data for determining the water vapor content spectroscopically (c_{Laser}) are given in Table 3. Each experiment's baseline signal ($I_{0,N2}$) is the average signal measured over a few minutes of flowing only nitrogen through the cell. This procedure was performed before each experiment MIX 1–3 and once before experiments MIX 4–6. The extinction coefficient ε_{H2O} results from the iterative solving procedure described in ***Section 2.3***. The uncertainties for ε_{H2O} and c_{Laser} include the spectrometer-related uncertainties in wave number determination and temperature measurement. A pressure of 1.013 bar in the cell is assumed for this measurement. Data used for determining $c_{Condensation}$ are also presented in Table 3. There is no uncertainty provided for this measurement for two reasons: First, the uncertainties in this process are primarily related to manual labor steps and, therefore, are not easily standardized. The uncertainties stem from handling and separation procedures, e.g., incomplete transfer of liquids between various equipment. Second, since there is a lack of established water vapor measuring procedures in gasification, this method has not been checked and validated against other methods in any studies.

The results from the condensation and spectroscopic measurements are combined with dry gas data to calculate the full gas composition in Fig. 8. The rest of the gas mixtures was N_2. The high uncertainties for c_{Laser} are rooted in the estimated temperature uncertainty inside the gas cell and the laser's wave number. These factors lead to uncertainty in calculating ε (Fig. 2) and, by extension, c_{Laser}. The data of both types of water vapor measurement fit well, especially considering the unknown accuracy of the condensation measurement. The average results for c_{Laser} are 4 – 18 % and for $c_{Condensation}$ 5 – 18 % below the target water vapor concentration. This negative deviation suggests that the pump likely delivered less than the target water flow rate. In conclusion, the spectroscopic setup provides results that agree with an established measurement over a wide range of H_2O concentrations and typical gas mixtures from gasification.

4.2. Second experimental campaign measuring raw and hot product gas from biomass steam gasification with advanced setup

The advanced spectroscopy setup was operated for around two hours during steam gasification of waste wood, and measurements were collected every 1 to 5 s. The baseline signal intensity in an N_2 atmosphere ($I_{0,N2}$) was measured as 5.71 mV at the lock-in amplifier before the experiment. The signal measured at the detector remained nearly constant during two hours of measuring hot and raw product gas from steady-state gasification. The average signal at the lock-in amplifier during the first hour of measurement was 2.03 mV, which is close to the average of 2.07 mV during the second hour. The baseline intensity $I_{0,N2}$ was used as a constant factor for calculating c_{Laser} by ***Eq. (2)*** during the experiment in real-time. The results of these calculations are shown in Fig. 9.

Fig. 9a shows the measurement uncertainty resulting from the margin of error for experimentally determining the laser wave number. The average difference over the two hours of gasification between $\nu = 76.44\ cm^{-1}$ and $\nu = 76.52\ cm^{-1}$ is rather small at 0.4 vol-%, while the difference between $\nu = 76.52\ cm^{-1}$ and $\nu = 76.60\ cm^{-1}$ is twice that at 0.8 vol-%. These results combine to a wavelength-uncertainty-related error of −0.4 to +0.8 vol-% H_2O. In the second campaign, the temperature was measured inside the cell by a Thermocouple type K with an error of ±1.5 °C. This improvement drastically reduces the temperature-related uncertainty, which is further helped by the decreased temperature sensitivity of this water vapor absorption line at temperatures between 220 – 400 °C (Fig. 1b). The resulting temperature-uncertainty-related error is around ±0.3 vol-% H_2O. The temperature and wavelength uncertainties combine to an estimated measuring error of

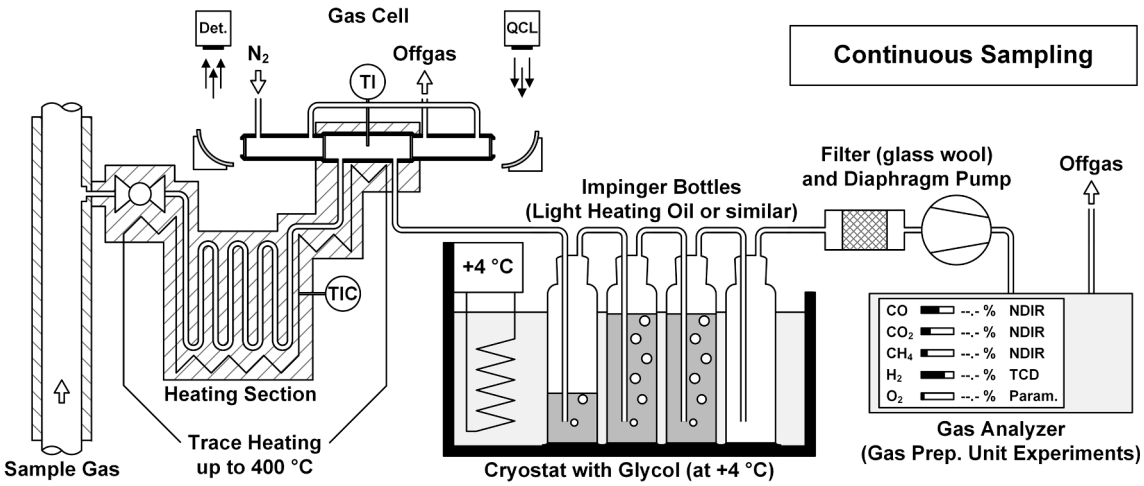

Fig. 7. Setup for the novel spectroscopic H_2O measurements, adjusted from [55]. Det. = Pyroelectric detector, QCL = THz quantum cascade laser.

Table 3
Results for experiments with synthetically prepared gas mixtures.

	Wave number ν	Temperature T	Average baseline signal $I_{0,N2}$	Average experimental signal I	Extinction coefficient ε_{H2O}	H_2O target	H_2O c_{Laser}	H_2O $c_{Condens.}$
	cm^{-1}	K	mV	mV	m^2/mol	vol-%	vol-%	vol-%
MIX 1	76.52 ± 0.08	383 ± 10	9.57	4.66	0.485 – 0.555	25.0	21.6 ± 1.5	22.8
MIX 2	76.52 ± 0.08	383 ± 10	10.62	8.30	0.378 – 0.445	10.0	9.3 ± 0.8	8.2
MIX 3	76.52 ± 0.08	383 ± 10	9.66	1.61	0.647 – 0.723	50.0	40.9 ± 2.6	46.5
MIX 4	76.52 ± 0.08	390 ± 10	5.73	1.38	0.593 – 0.663	42.5	35.9 ± 2.1	37.5
MIX 5	76.52 ± 0.08	388 ± 10	5.73	0.82	0.662 – 0.736	50.0	43.9 ± 2.5	47.6
MIX 6	76.52 ± 0.08	390 ± 10	5.73	1.57	0.576 – 0.644	35.0	33.6 ± 2.0	32.1

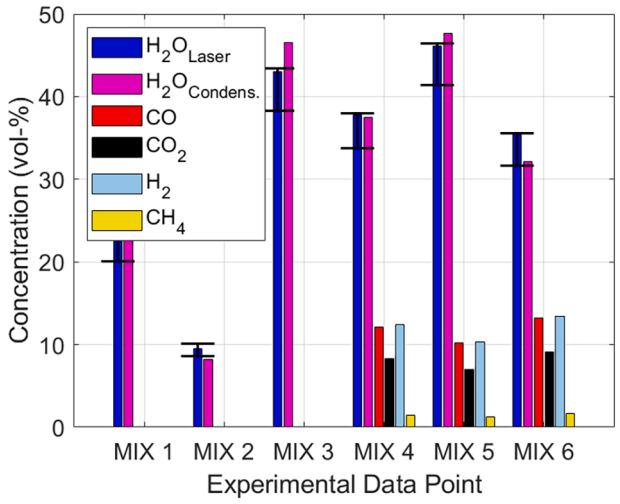

Fig. 8. Comparison of H_2O concentrations measured by condensation ($H_2O_{Condens.}$) and spectroscopy (H_2O_{Laser}) in various experiments with synthetically prepared gas mixtures.

−0.7 to +1.1 vol-% H_2O. This error margin substantially improved from the first campaign, which had higher uncertainties.

Fig. 9b shows the composition of the raw product gas over the experimental duration. The water vapor measurement results at the design wave number of $\nu = 76.52\ cm^{-1}$ were combined with the dry gas composition to give this raw gas composition. The average H_2O concentration for the condensation measurement, conducted from 10:27 to 10:39, was 46.7 vol-%. The spectroscopic measurement, on average, yielded 45.9 vol-%. Mass and energy balancing simultaneously calculated in the process simulation software IPSEpro suggested 44.6 – 45.3 vol-%. Over two hours, the average c_{Laser} result was 48.2 vol-%.

These measurements were performed in a raw product gas with H_2, CO_2, CO, CH_4, and N_2 as the main dry gas components. Of these components, only CO was suggested by the Spectral Calculator to influence the H_2O quantification in this QCL setup noticeably. Including CO measurement data from NDIR in the solving algorithm allowed for dynamically accounting for CO absorption. 15378 ppm NH_3 and 387 ppm H_2S were also found in the dry gas. While these species' absorption was not dynamically considered, the spectral calculator estimates their influence was low. Absorption values of 2E-03 for NH_3 and 9E-05 for H_2S were calculated, corresponding to an H_2O overestimation of 0.1 vol-%. This value can be used for calibration in post-processing, changing the spectroscopic measurement to 45.8 vol-% from 10:27 to 10:39 and 48.1 vol-% over the experimental duration. The total tar content in the raw product gas was determined as 31.21 g/Nm^3_{dry} by GC–MS, of which most were benzene and only 11.75 g/Nm^3_{dry} were not benzene, toluene, ethylbenzene, or xylenes (Appendix C). Gravimetric tar was determined as 4.18 g/Nm^3_{dry}. The tar dew point was calculated at 192 °C, suggesting that the temperature in the cell was sufficient to avoid tar condensation. This finding, the measurement's stability over two hours, and the comparison with the condensation measurement suggest that this novel device is well-equipped to handle tar-contaminated gases.

5. Discussion

This section discusses some possible errors that might have influenced the H_2O concentration results and how those errors could be reduced in future works.

Systematic errors are consistent and repeatable and occur due to flaws in the measurement system. This work used the simplification that the measurement signal at the lock-in amplifier is reduced from the

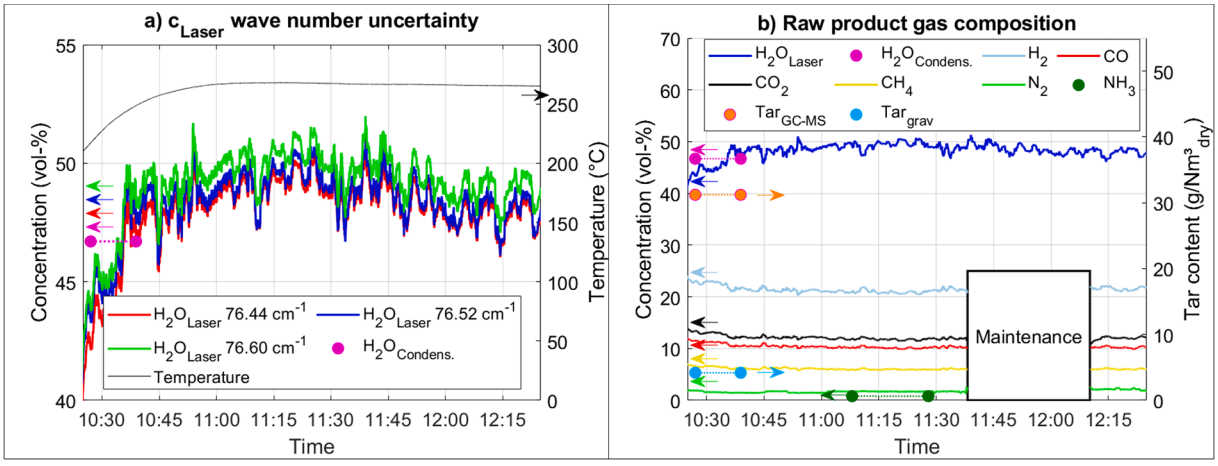

Fig. 9. H_2O measurement data for hot and raw product gas from biomass steam gasification. a) Uncertainty was introduced into water vapor measurement due to uncertainty in laser wave number, and b) Raw product gas composition data.

baseline signal only by absorption from H_2O and CO. Other effects that would reduce the baseline signal during measurement are neglected, which could lead to overestimating the H_2O content in the gas. Measurement data in this work and HITRAN2020 data are available for NH_3, H_2S, H_2, CO_2, and CH_4. H_2, CO_2, and CH_4 do not absorb significantly at 2.293 THz (see ***Section 2.1***). Data on NH_3 and H_2S abundance were unavailable as online measurements, but post-processing revealed that these species led to overestimating the H_2O concentration by 0.1 vol-%. If the setup was changed to allow for online measurement of NH_3 and H_2S, this error could be dynamically eliminated. The absorption from other components could not be considered since measurement or HITRAN2020 data were missing. An estimation for the maximum error during measurement can be given as the sum of errors induced by typical product gas impurities (see Table 1). If every impurity were present at its maximum considered concentration, this would result in a baseline decrease of around 5.1 %. At 250 °C, 1 atm, and ε_{H2O} of 0.5 m^2/mol, this would correspond to a maximal H_2O overestimation of 2.5 vol-%. This maximum error is primarily a result of absorption by 10 vol-% NH_3 and 0.1 vol-% HCN, which are very high numbers for biomass gasification. This estimation does not include the unknown absorption of any species for which data was unavailable in the HITRAN2020 database.

The baseline signal could also have been reduced through light scattering by particles or window fouling, possibly inducing another systematic error. The influence of these non-H_2O-absorption-losses could be investigated in future work. This investigation could include dedicated experimental campaigns measuring the impact of various components. Alternatively, other measurement techniques could be adopted, such as normalized wavelength modulation spectroscopy, which has been reported to reduce these errors [18,20]. Another systematic error results from using simulated lineshape profiles to calculate the molecular absorption coefficients. Voigt profiles typically show residuals within 2 % of measured lineshape around standard temperature and pressure but can be less accurate under certain circumstances [18].

Random errors arise from unpredictable fluctuations in the process. The conditions in the laboratory with the gasifier were not as controlled as in an optical laboratory and were representative field tests of a realistic application environment. Various machines, heat sources, people, and dust were close to the gasifier and spectroscopic setup; furthermore, the windows were open, and the laboratory was not air-conditioned. Under these laboratory conditions and without encasing the setup, the baseline signal intensity in an N_2 atmosphere ($I_{0,N2}$) was measured as 5.71 mV at the lock-in amplifier before the experiment. The signal-to-noise ratio was calculated as averaged signals versus the standard deviation σ of the transmitted signal. At $\sigma = 0.24$ mV, the resulting signal-to-noise ratio was 23.8 for the baseline signal. The signal-to-noise ratio was much lower at around 8 during actual measurement using the same standard deviation. Consequently, this means that very high H_2O content and correspondingly low signals at the lock-in-amplifier would have very low signal-to-noise ratios, a drawback of the employed fixed-frequency approach. Encasing the setup could increase the signal-to-noise ratio since the baseline and signal-to-noise ratios were higher in the optical laboratory. Additionally, encasing the setup would be necessary for more extended tests to exclude any absorption from ambient moisture and ensure that ambient moisture variation between the time of baseline measurement and experiment does not alter the results. A laser with a higher power output could also increase signal-to-noise ratios.

Dynamic errors occur when the measurement system cannot respond quickly to the measured quantity. In the context of gasification analysis, the repetition rates of the used electronic equipment are fast enough to avoid such errors. The computation interval for new measurements was somewhat arbitrarily chosen as “every few seconds”, sufficient for observing the product gas from a pilot-scale gasifier. One potential dynamic error occurs during temperature measurement in the cell by a thermocouple. The increase in c_{Laser} data near the start of the gasification experiment is not explained by a trend in the raw voltage signal at the lock-in amplifier. Instead, this trend appears once the raw signal is combined with the gas cell temperature data. The temperature increase near the start is explained by a change in gas supply from nitrogen to hot and raw product gas less than three minutes before the condensation measurement. As a result, the gas temperature might have been underestimated before the setup’s temperature was stabilized. One solution for future experiments is to avoid switching between gas supplies at varying temperature levels this close to the measurement. Another solution could be to implement spectroscopy-based temperature measurement with a faster response time, e.g., as Sepman et al. showed [23].

Instrumental errors are inherent to the measuring instruments and can be reduced by regular maintenance and calibration. Temperature measurements are one of the two primary sources of uncertainty discussed and presented in this work. Integrating the thermocouple directly into the cell helped to reduce this uncertainty considerably. The other prominently discussed uncertainty resulting from instrumental error is the laser frequency. The spectrometer’s resolution is defined by the path difference of the interferometer arms as $\pm$ 0.08 cm^{-1} and leaves some uncertainty when measuring the laser wavelength. This uncertainty is mainly due to the laser’s emitted frequency depending on the laser’s temperature. Consequently, refined measuring and stabilizing procedures for the laser’s temperature could reduce this uncertainty. These instrumental errors induced an error of −0.7 to +1.1 vol-% H_2O in this work.

A total estimation of measurement error can be given as the sum of partial errors that could be quantified. These errors include misclassifying absorption by other gases as absorption by H_2O and temperature- and wavelength-uncertainty-related errors. If all impurities listed in Table 1 were assumed to be unknown, the error would be increased to −3.2 to +1.1 vol-% H_2O. Consequently, careful consideration should be given to the NH_3 and HCN content if nitrogen-rich feedstocks are combined with this measurement. The absorption by other components, including those not listed in the HITRAN2020 database, remains unknown. Future works should aim to investigate the baseline variability resulting from absorption and scattering.

The measured water vapor contents are plausible for biomass steam gasification [52], although higher than expected if the water–gas shift reaction were in equilibrium at these operating conditions. The high value is likely a result of TUW operating their DFB gasification process with excess steam to achieve the desired superficial gas velocity for fluidization. This measurement could be used to optimize the steam ratio in future campaigns. The results from the new laser measurements are within the uncertainty calculated for the new measurement in this section compared to the discontinuous concentration measurement and mass balance. The excellent agreement between these results highlights the potential of this technology as a reliable online measurement that can improve process understanding and control for processes with complex gas mixtures.

6. Conclusion and outlook

This study introduced a novel spectroscopic device, including a quantum cascade laser emitting at 2.294 THz, a hot gas cell, and a pyroelectric detector to quantitatively measure H_2O in hot and raw product gas from biomass gasification. This design was chosen based on absorption data from the HITRAN2020 database calculated in the Spectral Calculator by GATS. Elevated temperatures of around 250 °C facilitated water vapor quantification without tar condensation impeding the measurement. The second campaign successfully adopted an advanced gas cell design at around 250 °C to avoid tar condensation and operate without interruption for two hours. The water vapor was embedded in a mixture that contained H_2, CO_2, CO, CH_4, N_2, NH_3, H_2S, and tar. Tar content in the raw product gas from steady-state gasification was determined as 31.21 g/Nm^3_{dry} by GC–MS and 4.18 g/Nm^3_{dry} gravimetrically. The average signal at the lock-in amplifier during the first hour of measurement was 2.03 mV, which is close to the average of

2.07 mV during the second hour of steady-state gasification. These results show that this technology can be used for hot and raw gases, including mixtures of permanent gases and uncondensed tar.

The measurements by QCL yielded results that were close to the results from offline analysis by condensation. When measuring raw product gas from biomass steam gasification, the condensation measurement showed 46.7 vol-%, while the spectroscopic measurement, on average, yielded 45.8 vol-%, and mass balancing suggested 44.6 – 45.3 vol-%. Both the condensation and the mass balancing results are within the uncertainty calculated for the spectroscopic measurement, which was −0.7 to +1.1 vol-% H_2O. The new laser method also provided preliminary results every 1 to 5 s in real-time, starkly contrasting the established condensation procedure, which produces average data for a given timespan and incurs a labor-related delay. Over two hours, the average c_{Laser} result was 48.1 vol-%. These points underscore that fixed-wavelength direct absorption using a QCL emitting in the far-infrared range is a promising option for water vapor quantification in harsh environments.

Further temperature and gas composition screenings and validation campaigns could reinforce the findings of this study and help with potential applications outside of biomass gasification. A limitation of this work is the uncertainty in laser frequency, which was a primary source of water vapor content uncertainty in measurement and is increasingly problematic at low water vapor contents and high temperatures in the gas cell. This uncertainty is primarily due to the laser's emitted frequency depending on the laser's temperature. Consequently, refined measuring and stabilizing procedures for the laser's temperature could reduce this uncertainty. Furthermore, the baseline variability in various gas mixtures should be investigated in future work. Signal-to-noise ratios could likely be increased by encasing the setup. Wavelength modulation spectroscopy could be considered to improve sensitivity and resistance against noise. The heating and insulation setup could also be further improved to avoid a drop in cell temperature when switching from cold to hot gas feeds.

CRediT authorship contribution statement

Florian Johann Müller: Writing – review & editing, Writing – original draft, Visualization, Software, Project administration, Methodology, Investigation, Formal analysis, Data curation, Conceptualization. **Michael Jaidl:** Writing – review & editing, Writing – original draft, Visualization, Software, Project administration, Methodology, Investigation, Data curation, Conceptualization. **Dominik Theiner:** Writing – review & editing, Software, Investigation, Data curation. **Johann Zeitlhofer:** Writing – review & editing, Writing – original draft, Visualization, Methodology, Investigation. **Florian Benedikt:** Writing – review & editing, Writing – original draft, Resources, Project administration, Investigation. **Lena Steiner:** Writing – review & editing, Writing – original draft, Investigation. **Alexander Bartik:** Writing – review & editing, Writing – original draft, Visualization, Resources, Project administration, Investigation, Funding acquisition. **Marie Christine Ertl:** Writing – review & editing. **Aaron Maxwell Andrews:** Writing – review & editing. **Gottfried Strasser:** Supervision, Resources, Funding acquisition. **Stefan Müller:** Writing – review & editing, Supervision, Resources, Funding acquisition. **Franz Winter:** Writing – review & editing, Supervision, Resources, Funding acquisition. **Karl Unterrainer:** Writing – review & editing, Supervision, Resources, Funding acquisition.

Declaration of competing interest

The authors declare that they have no known competing financial interests or personal relationships that could have appeared to influence the work reported in this paper.

Acknowledgments

This study was carried out within the doctoral college CO_2 Refinery at TU Wien and is supported by the ERA-NET Bioenergy project Bio-HEAT (FO999889752), funded by the Austrian Climate and Energy Fund. The authors acknowledge TU Wien Bibliothek for financial support through its Open Access Funding Programme. The authors would also like to thank Fabian Dona and Thomas Pareihs for manufacturing the laser cell, the Test Laboratory for Combustion Systems at TU Wien for the analytical measurements and everyone who contributed to the preparation and operation of the gasifier experiment. The authors acknowledge financial support from the Austrian Science Fund FWF (TeraLearn P35932-N). A.M.A. acknowledges the support of the European Office of Aerospace Research and Development/Air Force Office of Scientific Research (EOARD/AFOSR No. FA8655-22-1-7170 and FA8655-23-1-7070), and the Austrian Research Promotion Agency (FFG) Project Green Sensing (No. 883941).

Appendix A. – Iterative solving algorithm

The molar extinction coefficient's dependence on the molar H_2O concentration means that ***Eq. (2)*** needs to be solved iteratively. For this reason, a solving algorithm is adopted to determine c_{Laser} by the following steps:

1. Initialization
   a. Create parametrized, quadratic fits for ε_{H2O} and ε_{CO} that depend on the temperature and molar concentration and are based on data from the Spectral Calculator. (Fig. 2)
   b. Use 10 vol-% as a first guess for c_{Laser} and the dry gas measurement data from NDIR as a first guess for c_{CO}.
   c. Use the baseline intensity in nitrogen atmosphere as starting guess for I_0.
2. Iteration loop
   a. Calculate new estimates for ε_{H2O} and ε_{CO} from the parametrized fits, using the measured gas temperature and the latest guess for c_{Laser} and c_{CO} as parameters.
   b. Calculate a new c_{Laser} from ***Eq. (2)*** using constant values for R (8.3144 J•mol^{-1}•K^{-1}), p (101325 Pa), d (0.086 m), the latest estimate for the baseline intensity I_0, real-time measurement data for the temperature T and experimental intensity I, and the latest estimate for ε_{H2O}.
   c. Calculate a new c_{CO} from the new c_{Laser} and dry gas composition data for CO from NDIR measurement.
   d. Calculate a new estimate for the baseline intensity I_0 from the latest c_{CO} and $I_{0,N2}$ data from ***Eq. (3)*** and ***Eq. (4)***, using the same constant values as in step 2b.
   e. Compare the new calculation of c_{Laser} from step 2b to the previous estimate of c_{Laser}: If the difference between the two latest estimates for c_{Laser} is smaller than 0.01 vol-%, then accept the latest c_{Laser} as the measurement result. Otherwise, repeat the iteration loop.

Appendix B. – Pictures of the setup

Information on the used equipment is also available in *Section 3.1*.

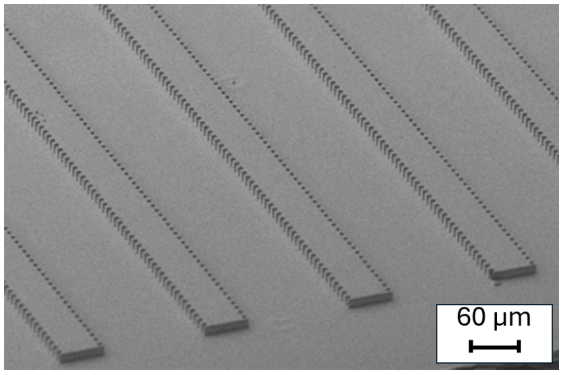

Fig. B1. Scanning electron microscope picture of ridge-type lasers with 1st-order distributed feedback grating for wavelength-selective single-mode emission

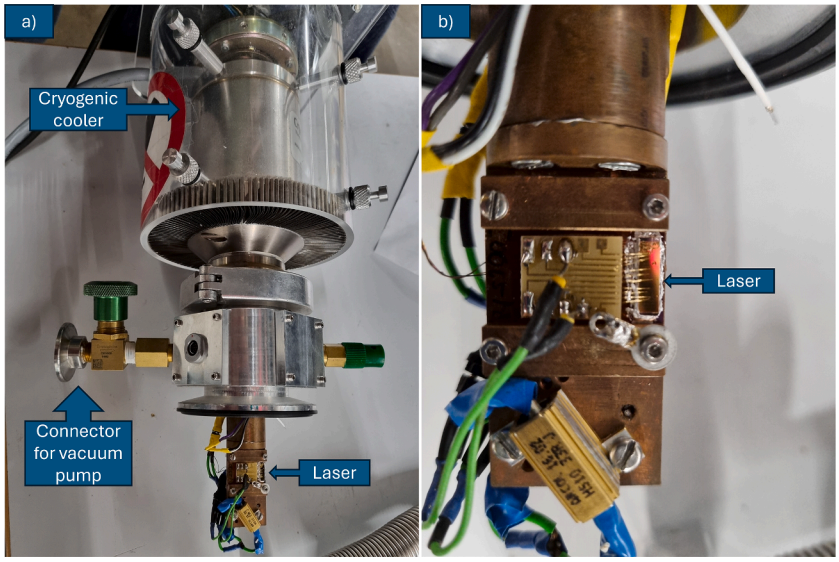

Fig. B2. Quantum cascade laser a) with cryogenic cooler, b) zoomed in

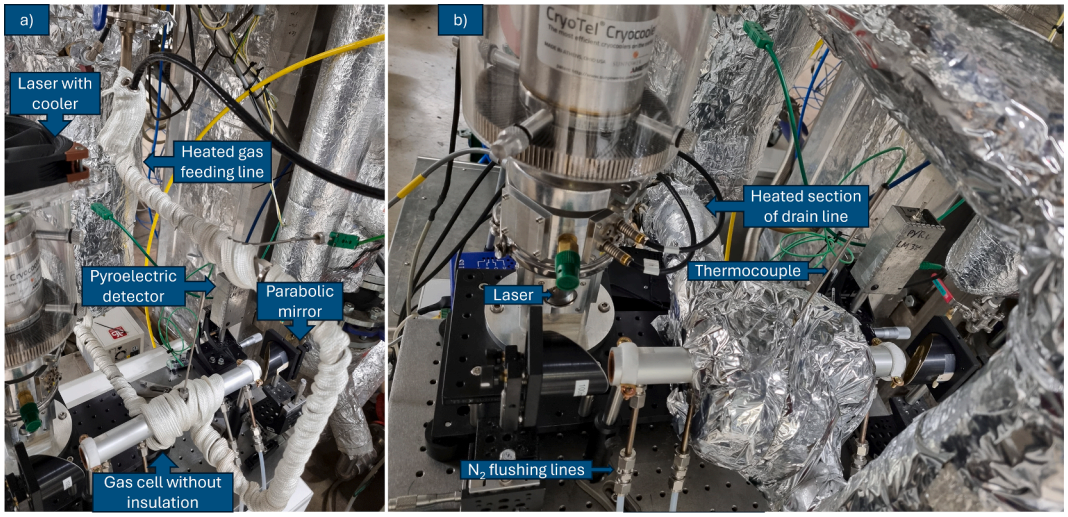

Fig. B3. Advanced gas cell setup: a) Without insulation, b) With insulation

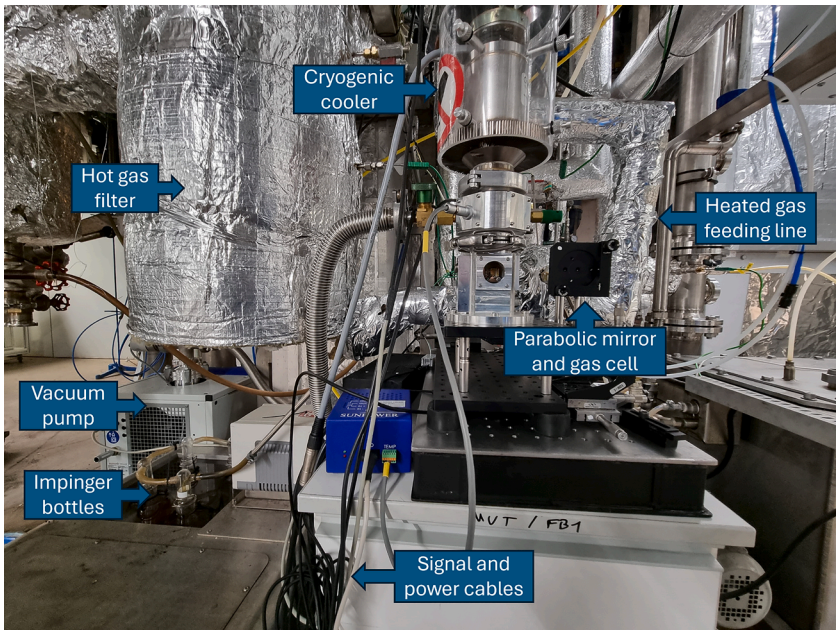

Fig. B4. Core gas cell setup including heated gas sampling line, quantum cascade laser, cryogenic cooler, parabolic mirror, gas drain line leading to Impinger bottles for condensation

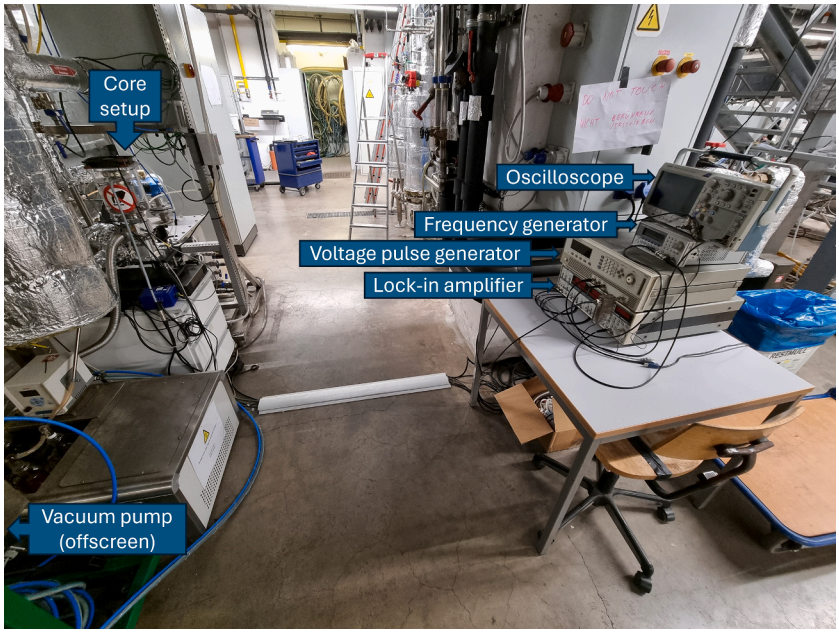

Fig. B5. Full setup including everything from Figure B- 4 and on the right table from top to bottom: oscilloscope, frequency generator (Agilent 33220A), voltage pulse generator (Agilent 8114A), lock-in amplifier (Stanford Research SR830)

Appendix C. – Detailed tar analysis

This tar analysis was conducted by GC–MS in the Testing Laboratory for Combustion Systems at Technische Universität Wien. The tar dew point for this mixture was estimated as 192 °C from vapor/liquid equilibrium calculations for single components [56], followed by the application of Raoult's law [57].

Table C1. Tar compound analysis via GC–MS. "n.m."=not measured.

Compound	Concentration	Compound	Concentration
	mg/Nm^3_{dry}		mg/Nm^3_{dry}
Benzene	19,459	Indole	
Toluene	n.m.	Biphenyl	197
2-Methylpyridine	n.m.	1-Vinylnaphthalene	n.m.

(*continued on next page*)

(*continued*)

Compound	Concentration	Compound	Concentration
Ethylbenzene	n.m.	2-Vinylnaphthalene	61
m- and p-Xylene	n.m.	Isoeugenol	n.m.
o-Xylene + Styrene	464	Acenaphthylene	1433
Phenylacetylene	n.m.	Acenaphthene	57
3- and 4-Methylpyridine	n.m.	Dibenzofuran	n.m.
Mesitylene	n.m.	Fluorene	415
Phenol	42	Dibenzothiophene	n.m.
Benzofuran	n.m.	Anthracene	389
1H-Indene	1053	Phenanthrene	1365
2-Methylphenol	<19.93	Carbazole	n.m.
3- and 4-Methylphenol	<19.93	4,5-Methylenephenanthrene	n.m.
2-Methylbenzofuran	n.m.	9-Methylanthracene	n.m.
2,6-Dimethylphenol	n.m.	Fluoranthene	585
2,5- and 2,4-Dimethylphenol	n.m.	Pyrene	375
3,5-Dimethylphenol	n.m.	Benzo[a]anthracene	120
2,3-Dimethylphenol	n.m.	Chrysene	120
3,4-Dimethylphenol	n.m.	Benzo[b]fluoranthene	95
2-Methoxy-4-Methylphenol	n.m.	Benzo[k]fluoranthene	37
Naphthalene	4552	Benzo[e]pyrene	85
1-Benzothiophene	n.m.	Benzo[a]pyrene	n.m.
Quinoline	n.m.	Perylene	<19.93
2-Methylnaphthalene	172	Dibenz[a,h]anthracene	<19.93
Isoquinoline	n.m.	Benzo[g,h,i]perylene	23
1-Methylnaphthalene	75	Indeno[1,2,3-cd]pyrene	35
1-Indanone	n.m.	Anthanthrene	n.m.
Eugenol	n.m.	Coronene	<19.93

Data availability

Data will be made available on request.

References

[1] Lee H, Calvin K, Dasgupta D, Krinner G, Mukherji A, Thorne PW, et al. Climate Change 2023: Synthesis Report. Contribution of Working Groups I, II and III to the Sixth Assessment Report of the Intergovernmental Panel on Climate Change. Geneva, Switzerland: 2023. https://doi.org/10.59327/IPCC/AR6-9789291691647.

[2] Fawzy S, Osman AI, Doran J, Rooney DW. Strategies for mitigation of climate change: a review. Environ Chem Lett 2020;18:2069–94. https://doi.org/10.1007/s10311-020-01059-w.

[3] Pröll T, Zerobin F. Biomass-based negative emission technology options with combined heat and power generation. Mitig Adapt Strateg Glob Chang 2019;24:1307–24. https://doi.org/10.1007/s11027-019-9841-4.

[4] Williams CL, Westover TL, Emerson RM, Tumuluru JS, Li C. Sources of biomass feedstock variability and the potential impact on biofuels production. Bioenergy Res 2016;9:1–14. https://doi.org/10.1007/s12155-015-9694-y.

[5] Molino A, Chianese S, Musmarra D. Biomass gasification technology: the state of the art overview. J Energy Chem 2016;25:10–25. https://doi.org/10.1016/j.jechem.2015.11.005.

[6] Gruber H, Groß P, Rauch R, Reichhold A, Zweiler R, Aichernig C, et al. Fischer-Tropsch products from biomass-derived syngas and renewable hydrogen. Biomass Convers Biorefin 2021;11:2281–92. https://doi.org/10.1007/s13399-019-00459-5.

[7] Bartik A, Benedikt F, Fuchs J, Hofbauer H, Müller S. Experimental investigation of hydrogen-intensified synthetic natural gas production via biomass gasification: a technical comparison of different production pathways. Biomass Convers Biorefin 2023. https://doi.org/10.1007/s13399-023-04341-3.

[8] Gubin V, Benedikt F, Thelen F, Hammerschmid M, Popov T, Hofbauer H, et al. Hydrogen production from woody biomass gasification: a techno-economic analysis. Biofuels Bioprod Biorefin 2024;1:1–19. https://doi.org/10.1002/bbb.2647.

[9] Rauch R, Hrbek J, Hofbauer H. Biomass gasification for synthesis gas production and applications of the syngas. Adv Bioenergy: Sustainab Challenge 2015:73–91. https://doi.org/10.1002/9781118957844.CH7.

[10] Benedikt F, Kuba M, Schmid JC, Müller S, Hofbauer H. Assessment of correlations between tar and product gas composition in dual fluidized bed steam gasification for online tar prediction. Appl Energy 2019;238:1138–49. https://doi.org/10.1016/j.apenergy.2019.01.181.

[11] Thunman H, Seemann M. The gobigas plant. substitute natural gas from waste: technical assessment and industrial applications of biochemical and thermochemical processes. Elsevier 2019:455–74. https://doi.org/10.1016/B978-0-12-815554-7.00017-9.

[12] Hofbauer H, Rauch R. Stoichiometric Water Consumption of Steam Gasification by the FICFB-Gasification Process. Progress in Thermochemical Biomass Conversion (Vol.1), Blackwell Science Ltd; 2001, p. 199–208.

[13] Veress M. Optimization of a process concept for the industrial production of Bio-SNG from low-grade fuels. Master Thesis Technische Universität Wien 2020. https://doi.org/10.34726/hss.2020.63703.

[14] DIN Deutsches Institut für Normung e.V. Biomass gasification - tar and particles in product gas - sampling and analysis: DIN CEN/TS 15439 2006.

[15] IEA Bioenergy. Gas analysis in gasification of biomass and waste - Guideline Report - Document 1. 2018.

[16] Kleinhappl M. Water measurement; an introduction. Webinar Presentation 2014.

[17] IEA. Gas analysis in gasification of biomass and waste Guideline Report - Document 2 - Factsheets on gas analysis techniques. 2018.

[18] Goldenstein CS, Spearrin RM, Jeffries JB, Hanson RK. Infrared laser-absorption sensing for combustion gases. Prog Energy Combust Sci 2017;60:132–76. https://doi.org/10.1016/j.pecs.2016.12.002.

[19] Bolshov MA, Kuritsyn YA, Romanovskii YV. Tunable diode laser spectroscopy as a technique for combustion diagnostics. Spectrochim Acta Part B at Spectrosc 2015;106:45–66. https://doi.org/10.1016/j.sab.2015.01.010.

[20] Salazar DV, Goldenstein CS, Jeffries JB, Seiser R, Cattolica RJ, Hanson RK. Design and implementation of a laser-based absorption spectroscopy sensor for in situ monitoring of biomass gasification. Meas Sci Technol 2017;28. https://doi.org/10.1088/1361-6501/aa8cf6.

[21] Lu F, Cao Z, Chang L, Zhao K, Xue X, Lin Y, et al. Precise velocity measurement by using even-symmetric 2f/1f harmonics extracted from up- and down-scanning WMS signal. IEEE Trans Instrum Meas 2024;73:1–11. https://doi.org/10.1109/TIM.2024.3470052.

[22] Sepman A, Ögren Y, Gullberg M, Wiinikka H. Development of TDLAS sensor for diagnostics of CO, H_2O and soot concentrations in reactor core of pilot-scale gasifier. Appl Phys B 2016;122:1–12. https://doi.org/10.1007/s00340-016-6319-x.

[23] Sepman A, Ögren Y, Qu Z, Wiinikka H, Schmidt FM. Real-time in situ multi-parameter TDLAS sensing in the reactor core of an entrained-flow biomass gasifier. Proc Combust Inst 2017;36:4541–8. https://doi.org/10.1016/j.proci.2016.07.011.

[24] Sepman A, Fredriksson C, Ögren Y, Wiinikka H. Laser-based, optical, and traditional diagnostics of no and temperature in 400 kw pilot-scale furnace. Appl Sci (switzerland) 2021;11. https://doi.org/10.3390/app11157048.

[25] Sepman A, Wennebro J, Fernberg J, Wiinikka H. Following fuel conversion during biomass gasification using tunable diode laser absorption spectroscopy diagnostics. Fuel 2024;374:132374. https://doi.org/10.1016/j.fuel.2024.132374.

[26] Sur R, Sun K, Jeffries JB, Hanson RK, Pummill RJ, Waind T, et al. TDLAS-based sensors for in situ measurement of syngas composition in a pressurized, oxygen-blown, entrained flow coal gasifier. Appl Phys B 2014;116:33–42. https://doi.org/10.1007/s00340-013-5644-6.

[27] De JW, Hein KRG. Nitrogen compounds in pressurised fluidised bed gasification of biomass and fossil fuels. Technical University Delft; 2005. PhD thesis.

[28] Xu J, He Q, Xiong Z, Yu Y, Zhang S, Hu X, et al. Raman spectroscopy as a versatile tool for investigating thermochemical processing of coal, biomass, and wastes: Recent advances and future perspectives. Energy Fuel 2021;35:2870–913. https://doi.org/10.1021/acs.energyfuels.0c03298.

[29] Wu J, Deng K-L, Guida R, Lee BK. Fiber-optic photo-acoustic spectroscopy sensor for harsh environment gas detection. Proc.SPIE, vol. 6698, 2007, p. 66980E. https://doi.org/10.1117/12.734092.

[30] Bidgoli H, Cherednichenko S, Nordmark J, Thunman H, Seemann M. Terahertz spectroscopy for real-time monitoring of water vapor and CO levels in the producer gas from an industrial biomass gasifier. IEEE Trans Terahertz Sci Technol 2014;4:722–33. https://doi.org/10.1109/TTHZ.2014.2357344.
[31] Vogler J, Stanger L, Bartik A, Schirrer A, Kozek M. Soft Sensor Design for Product Gas Composition Monitoring Including Fault Isolation in a Dual Fluidized Bed Biomass Gasifier. 2024 International Conference on Control, Automation and Diagnosis (ICCAD), IEEE; 2024, p. 1–6. https://doi.org/10.1109/ICCAD60883.2024.10553785.
[32] Suzuki EM, Buzzing P. Applications of Raman spectroscopy in forensic science. I: Principles, comparison to infrared spectroscopy, and instrumentation. Forensic Sci Rev 2018;30:111–35.
[33] Eichmann SC, Kiefer J, Benz J, Kempf T, Leipertz A, Seeger T. Determination of gas composition in a biogas plant using a Raman-based sensorsystem. Meas Sci Technol 2014;25. https://doi.org/10.1088/0957-0233/25/7/075503.
[34] Karellas S, Karl J. Analysis of the product gas from biomass gasification by means of laser spectroscopy. Opt Lasers Eng 2007;45:935–46. https://doi.org/10.1016/j.optlaseng.2007.03.006.
[35] Ge H, Sun Z, Jiang Y, Wu X, Jia Z, Cui G, et al. Recent Advances in THz Detection of Water. Int J Mol Sci 2023;24. https://doi.org/10.3390/ijms241310936.
[36] Song Y, Wang Z, Loh J, Thomson MJ. High-Temperature H2O Vapor Measurement Using Terahertz Spectroscopy for Industrial Furnace Applications. IEEE Trans Terahertz Sci Technol 2016;6:26–31. https://doi.org/10.1109/TTHZ.2015.2503702.
[37] Sudiarta IW, Chýlek P. Mie scattering by a spherical particle in an absorbing medium. Appl Opt 2002;41:3545. https://doi.org/10.1364/ao.41.003545.
[38] Wang Y, Zhao P, Gao W, Chen X. Optimization of forward-scattered light energy and de-coherence of Mie scattering for speckle suppression. Opt Quantum Electron 2015;47:235–46. https://doi.org/10.1007/s11082-014-9907-1.
[39] Köhler R, Tredicucci A, Beltram F, Beere HE, Linfield EH, Davies AG, et al. Terahertz semiconductor-heterostructure laser. Nature 2002;417:6885. 2002;417:156–9. https://doi.org/10.1038/417156a.
[40] GATS. Calculation of molecular spectra with the Spectral Calculator 1994:1–15.
[41] Gordon IE, Rothman LS, Hargreaves RJ, Hashemi R, Karlovets EV, Skinner FM, et al. The HITRAN2020 molecular spectroscopic database. J Quant Spectrosc Radiat Transf 2022;277:107949. https://doi.org/10.1016/j.jqsrt.2021.107949.
[42] Gordley LL, Marshall BT, Allen CuD. Linepak: Algorithms for modeling spectral transmittance and radiance. J Quant Spectrosc Radiat Transf 1994;52:563–80. https://doi.org/10.1016/0022-4073(94)90025-6.
[43] De S, Agarwal AK, Moholkar VS, Thallada B. Coal and Biomass Gasification. 1st ed. Singapore: Springer; 2018. https://doi.org/10.1007/978-981-10-7335-9.
[44] Benedikt F. Fuel flexible advanced dual fluidized bed steam gasification. Dissertation Technische Universität Wien 2020. https://doi.org/10.34726/hss.2020.39988.
[45] Karl J, Pröll T. Steam gasification of biomass in dual fluidized bed gasifiers: a review. Renew Sustain Energy Rev 2018;98:64–78. https://doi.org/10.1016/j.rser.2018.09.010.
[46] Mauerhofer AM, Müller S, Bartik A, Benedikt F, Fuchs J, Hammerschmid M, et al. Conversion of CO_2 during the DFB biomass gasification process. Biomass Convers Biorefin 2021;11:15–27. https://doi.org/10.1007/s13399-020-00822-x.
[47] Müller FJ, Fuchs J, Müller S, Winter F. CO_2 conversion to CO by fluidized bed biomass gasification: Measuring CO_2 utilization via stable carbon isotope ratios. J CO2 Util 2024;83. https://doi.org/10.1016/j.jcou.2024.102792.
[48] GATS. Spectral Calculator-Hi-resolution gas spectra 2023. https://www.spectralcalc.com/calc/spectralcalc.php (accessed August 17, 2023).
[49] Amanti MI, Scalari G, Terazzi R, Fischer M, Beck M, Faist J, et al. Bound-to-continuum terahertz quantum cascade laser with a single-quantum-well phonon extraction/injection stage. New J Phys 2009;11. https://doi.org/10.1088/1367-2630/11/12/125022.
[50] Williams BS, Kumar S, Hu Q, Reno JL. Distributed-feedback terahertz quantum-cascade lasers with laterally corrugated metal waveguides. Opt Lett 2005;30:2909. https://doi.org/10.1364/OL.30.002909.
[51] Kaltschmitt M, Hofbauer H, Lenz V. Energie aus Biomasse. 4th ed. Wiesbaden: Springer Fachmedien Wiesbaden; 2024. https://doi.org/10.1007/978-3-658-41216-6.
[52] Schmid JC, Benedikt F, Fuchs J, Mauerhofer AM, Müller S, Hofbauer H. Syngas for biorefineries from thermochemical gasification of lignocellulosic fuels and residues—5 years' experience with an advanced dual fluidized bed gasifier design. Biomass Convers Biorefin 2021;11:2405–42. https://doi.org/10.1007/s13399-019-00486-2.
[53] GeoSphere Austria. Messstationen Stundendaten v2 2024. https://doi.org/10.60669/9bdm-yq93.
[54] Wilk V. Extending the range of feedstock of the dual fluidized bed gasification process towards residues and waste. Dissertation Technische Universität Wien 2013.
[55] Kern S, Pfeifer C, Hofbauer H. Gasification of wood in a dual fluidized bed gasifier: influence of fuel feeding on process performance. Chem Eng Sci 2013;90:284–98. https://doi.org/10.1016/j.ces.2012.12.044.
[56] Rabou LPLM, Zwart RWR, Vreugdenhil BJ, Bos L. Tar in biomass producer gas, the Energy research Centre of The Netherlands (ECN) experience: An enduring challenge. Energy Fuel 2009;23:6189–98. https://doi.org/10.1021/ef9007032.
[57] Thersites: Tar dew point n.d. https://www.thersites.nl/tardewpoint.aspx (accessed September 4, 2024).